PHYSICAL REVIEW A **84**, 021801(R) (2011)

Heterodyne coherent anti-Stokes Raman scattering by the phase control of its intrinsic background

Xi Wang,* Kai Wang, George R. Welch, and Alexei V. Sokolov

Department of Physics and Institute of Quantum Science and Engineering, Texas A&M University, College Station, Texas 77843-4242, USA

(Received 22 February 2011; published 5 August 2011)

We demonstrate the use of femtosecond laser pulse shaping for precise control of the interference between the coherent anti-Stokes Raman scattering (CARS) signal and the coherent nonresonant background generated within the same sample volume. Our technique is similar to heterodyne detection with the coherent background playing the role of the local oscillator field. In our experiment, we first apply two ultrashort (near-transform-limited) femtosecond pump and Stokes laser pulses to excite coherent molecular oscillations within a sample. After a short and controllable delay, we then apply a laser pulse that scatters off of these oscillations to produce the CARS signal. By making fine adjustments to the probe field spectral profile, we vary the relative phase between the Raman-resonant signal and the nonresonant background, and we observe a varying spectral interference pattern. These controlled variations of the measured pattern reveal the phase information within the Raman spectrum.

DOI: 10.1103/PhysRevA.84.021801 PACS number(s): 42.65.Dr, 42.25.Hz, 42.30.Rx, 42.65.Re

Coherent anti-Stokes Raman scattering (CARS) spectroscopy is a powerful technique which combines high sensitivity with inherent chemical selectivity [1]. CARS occurs when molecules of interest, coherently excited by light pulses, scatter laser light to produce spectral components shifted by the molecular oscillation frequencies. Briefly, CARS is a third-order nonlinear process, involving three incident pulses: pump, Stokes, and probe, with respective frequencies ω_p, ω_S, and ω_{pr}. When the frequency difference between the pump pulse and the Stokes pulse ($\omega_p - \omega_S$) matches the molecular vibrational frequency of the sample, the CARS signal is produced at a blueshifted frequency of the probe ($\omega_p - \omega_S + \omega_{pr}$). Chemical selectivity is afforded by the species-specific molecular vibrational spectra, and sensitivity is enhanced due to the coherent nature of the scattering process [2,3]. However, CARS spectroscopy is often hindered by the presence of a strong background which is due to coherent nonresonant four-wave mixing (FWM).

The FWM background is usually considered as a detriment to CARS. When this background is large, its inevitable random fluctuations obscure the CARS signal. Many clever techniques have been devised to suppress the background [4–9]. Of particular relevance to our present work is the optimized CARS scheme where background suppression is accomplished by shaping and delaying the probe laser pulse such that it has zero temporal overlap with the pump and Stokes pulses [10,11]. In the work presented here, instead of eliminating the FWM background completely, we control it in such a way as to enhance the CARS signal. We use the FWM field as a local oscillator (LO) for heterodynelike phase-sensitive signal detection and amplification. Our technique is based on breaking the symmetry of the probe spectrum and thereby introducing a gradual phase change of the probe field versus time. Then, by exploiting the difference in the time response of the (instantaneous) FWM and the (time-accumulated) resonant Raman signal, we control the relative phase between the signal and LO fields.

Heterodyne CARS has been successfully applied in the past [12–16]; however, it requires elaborate interferometric setups where the local oscillator field is generated (typically by FWM) in one arm of an interferometer, while the CARS signal is produced in the other arm. We show here how both CARS (signal) and FWM (LO) fields can be produced simultaneously, *in situ* within the same sample volume, using proper pulse shaping, described below, to allow their relative phase to be precisely controlled. The idea to control the phase was also proposed in Refs. [17,18] based on pulse shaping.

The experimental setup in Fig. 1 is adapted from our previous optimized CARS technique [12]. The pump (central wavelength at 1295 nm and FWHM 50 nm) and Stokes (1500 nm, FWHM 70 nm) beams are broadband, near-Gaussian, femtosecond pulses, and the probe has a top-hat-like spectrum with a relatively narrow bandwidth (800 nm, FWHM of around 1 nm) obtained with a pulse shaper, as shown in Fig. 1(b). Their schematic temporal profiles are shown in the inset of Fig. 1(a).

The three beams have parallel polarization and are collinearly overlapped in space with pulse energies of a few hundred nanojoules. The pump and Stokes pulses are also overlapped in the time domain, and the probe pulse can be delayed by a computer-controlled translation stage with a step resolution of 1 μm. The signal is collected by a spectrograph and a liquid nitrogen-cooled CCD (Princeton Instrument, Spec-10:400BR/LN) with an exposure time of 200 ms. We use methanol aqueous solution as the sample since methanol has an individual Raman line at around 1040 cm^{-1}. The solution is held in a 2-mm-thick fused silica cell with a concentration of around 10% by volume ($\approx$2.5 M) to make the resonant and nonresonant fields comparable.

Figure 1(c) shows two different probe spectra with opposite and unequal asymmetries. The probe spectrum taken without inserting the knife edge into the pulse shaper [blue dotted curve in Fig. 1(c)] is slightly less intense at shorter wavelengths. Inserting a knife edge into the pulse shaper (before the focus occurring at the slit) produces a spectrum that is less intense at longer wavelengths [green solid curve in Fig. 1(c)]. In the time domain, the probe fields are sinclike in both cases, but with nonzero nodes as shown in Figs. 3(a) and 3(b), which are

*xwangphy@gmail.com

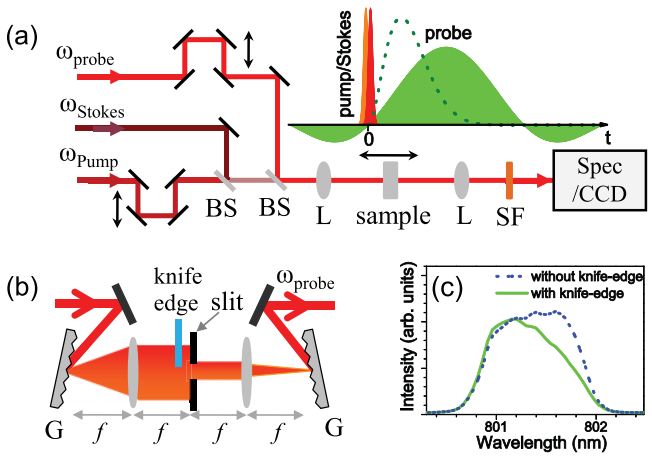

FIG. 1. (Color online) (a) Schematic of the collinear CARS setup; the inset shows temporal ranges and profiles of the pump, Stokes, and probe beams. The dotted curve shows the resonant contribution of the probe field versus time. (b) $4f$ pulse shaper used to produce a top-hat-like probe spectrum; a knife edge can be placed in front of the focal plane to make the spectrum (more) asymmetric. (c) Measured probe spectra without (blue dotted) and with (green solid) the knife edge. BS, beam splitter; L, lens; Spec, spectrograph; G, grating; SF, short-pass filter.

obtained from the same setup by measuring the FWM from the cell while changing the probe delay.

The third-order polarization for the CARS generation is the sum of the background (BG) and resonant contributions

$$P^{(3)}_{\mathrm{CARS}} = P^{(3)}_{\mathrm{BG}}(\omega,\tau) + P^{(3)}_{R}(\omega,\tau) = \int_0^\infty d\Omega\left[\chi^{(3)}_{\mathrm{BG}}(\Omega) + \chi^{(3)}_{R}(\Omega)\right] E_{pr}(\omega-\Omega,\tau)\, R(\Omega), \tag{1}$$

where $R(\Omega) = \int_0^\infty E_p(\omega')E_S(\omega'-\Omega)d\omega'$; $E_{pr}(\omega,\tau)$, $E_p(\omega)$, and $E_S(\omega)$ are the probe, pump, and Stokes fields, respectively [10,19], and τ is the time delay of the probe peak relative to the preparatory pulses (pump and Stokes) which overlap in time (defined as $t = 0$). Most often $\chi^{(3)}_{\mathrm{BG}}$ corresponds to nonresonant FWM response and is purely real, while $\chi^{(3)}_{R}$ is complex and typically Lorentzian. In the current work, we introduce asymmetry into the probe spectrum by pulse shaping and hence create a complex FWM background $P^{(3)}_{\mathrm{BG}}(\omega,\tau)$ instead of a purely real one. If we define ϕ as the phase of the background, the total CARS signal can be written as

$$S_{\mathrm{CARS}} = \left|P^{(3)}_{\mathrm{BG}}\right|^2 + \left|P^{(3)}_{R}\right|^2 + 2\,\mathrm{Re}\left[e^{i\phi}\left|P^{(3)}_{\mathrm{BG}}(\omega,\tau)\right|P^{(3)*}_{R}(\omega,\tau)\right]. \tag{2}$$

In our experiment, the probe bandwidth is chosen to be somewhat smaller than the resonant Raman linewidth, therefore $P^{(3)}_{R}(\omega) \propto \chi^{(3)}_{R}(\omega)$. Since the FWM is broadband, i.e., insensitive to frequency, choosing $\phi = \pm\pi/2$, as an example, allows extraction of the imaginary part of $\chi^{(3)}_{R}$, which can be directly compared with spontaneous Raman spectra.

More generally, a variable ϕ allows the intrinsic FWM background to act as a LO in heterodyne detection. Our ability to adjust ϕ arbitrarily relies on the fact that the nonresonant FWM is an instantaneous process, so only the part of the probe pulse overlapping with the preparatory pulses at $t = 0$ contributes to the FWM, whereas the resonant Raman signal is an accumulation process due to the finite lifetime of the vibrational coherence, so the full duration of the probe when $t \geqslant 0$ contributes. In our configuration, the resonant contribution of the probe field at different moments can be described by the dotted curve in the inset of Fig. 1(a). We can see that the maximum of the curve occurs after the preparatory pulses, at a fairly large time delay (at around $t = \tau/2$). The total resonant Raman field is the integration of the entire area under the curve; therefore, the resonant signal including its phase will not be affected significantly when we vary the probe delay slightly. However, the phase of the FWM field is directly related to the instantaneous phase of the probe field at the overlap moment and thus is very sensitive to the probe delay.

For a temporally ideal sinc probe, the phase of the FWM will jump by π as the field changes sign at the node. This is what needs to be avoided for the heterodyne effect. We can accomplish this by making the probe somewhat asymmetric in frequency space so that the probe field has a nonzero imaginary part as the real part changes sign. This is illustrated in Fig. 2, where we show an example top-hat probe spectrum (black solid) with a Gaussian shoulder $e^{-(\omega+1)^2}$ at the low-frequency side and hyper-Gaussian shoulder $e^{-(\omega-1)^4}$ at the high-frequency side. (This is an example—the exact shapes are not so important since only the asymmetry is essential.) The corresponding temporal functions are shown in Figs. 2(b)–2(f). For comparison, Fig. 2 also shows the spectrum

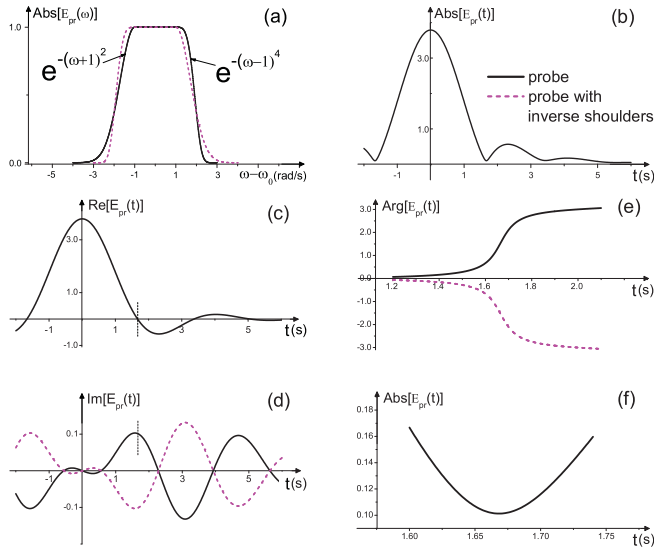

FIG. 2. (Color online) (a) The solid (black) curve is a slightly asymmetric top-hat probe field $E_p(\omega)$, and the dashed (magenta) curve is one with the opposite asymmetry. Both have hyper-Gaussian shoulders. (b)–(f) show the corresponding time-domain transforms corresponding to these two curves (black solid and magenta dashed, respectively). We show (b) the absolute value Abs$[E_{pr}(t)]$, (c) the real part Re$[E_{pr}(t)]$, (d) the imaginary part Im$[E_{pr}(t)]$, and (e) the argument Arg$[E_{pr}(t)]$ of the probe field in (a). (f) is a zoom of (b). Quantities plotted are dimensionless.

with shoulders of opposite asymmetry and the corresponding temporal functions in magenta (dashed). Their absolute values and real parts are the same, however, the signs of their imaginary parts are opposite.

As a result of the asymmetry, the argument ϕ of the complex probe field [black solid curve in Fig. 2(e)] will gradually shift from 0 to π as the real part of the field changes sign. This phenomenon is analogous to the (spatial) Gouy phase shift (by π) that occurs for a Gaussian beam as it evolves from $-\infty$ to $+\infty$ through a focus. For the spectrum with the opposite asymmetry, the argument changes from 0 to $-\pi$ [magenta dashed curve in Fig. 2(e)]. Furthermore, we also have the flexibility to modify the asymmetry so as to change the proportion of the imaginary to the real components, as shown by the actual spectra used in this experiment in Fig. 1(c). Thus, we can control both the relative phase and amplitude between the FWM and resonant signal. This key point allows the FWM itself to act as the LO field in heterodyne detection.

The study of the probe asymmetry is of practical interest, not only due to the self-implemented heterodyne effect discussed above. We have succeeded in eliminating the FWM background in our previous work [10]. However, properly introducing some background benefits the detection sensitivity as well [11]. Because it is impractical to produce a perfectly symmetric spectrum in an experiment, this study gives a useful understanding of how this type of optimized CARS works, especially for samples with low concentrations where a small amount of FWM may dominate over the signal being sought.

Figure 3 shows the measured CARS spectra of methanol aqueous solution near the first probe nodes without (left column) and with knife edge (right column). In order to highlight the feature of the Raman line, the spectra in Figs. 3(a)–3(d) are rescaled as $I_{\mathrm{CARS}}(\omega)/I_{\mathrm{BG}}(\omega)$, where $I_{\mathrm{BG}}(\omega)$ is obtained through fitting to the FWM background. In Figs. 3(a) and 3(b), we expressly point out that there is a distinct phase change by π between the two spectra (insets) slightly after the first probe node (indicated by the arrows, at 2.08 and 2.16 ps, respectively), and we attribute this to the opposite asymmetry of the probe spectra.

The phase-sensitive heterodyne effect is revealed by the gradual changes of the phases with probe delays shown in Figs. 3(c) and 3(d). The numbers in the graphs are the probe delays, marked as the black dots on the probe temporal shapes in Figs. 3(a) and 3(b). Obvious phase changes occur in both cases, especially in Fig. 3(d), where the phase changes approximately by π from $\tau = 1.68$ ps to $\tau = 2.16$ ps and a transition phase appears at $\tau = 2.08$ ps (the node). However, it is not quite straightforward to estimate the phase change in Fig. 3(c) since there is a considerable amount of resonant contribution $|P_R(\omega)|^2$. The opposite temporal evolutions of the CARS signal for these two cases are apparent from the contour graphs in Figs. 3(e) and 3(f), the CARS intensity spectrum as a function of probe delay. The contour graph helps to find the desired phase position for each probe spectral profile and here consists of 60 CARS spectra. When we compare Figs. 3(c) and 3(d), we can see that the spectra are fairly similar far from the nodes and quite different near the nodes. This result confirms the expectation from Fig. 2(e) where the phase difference from opposite spectral asymmetry reaches its maximum (π) at the node and decreases away from the node.

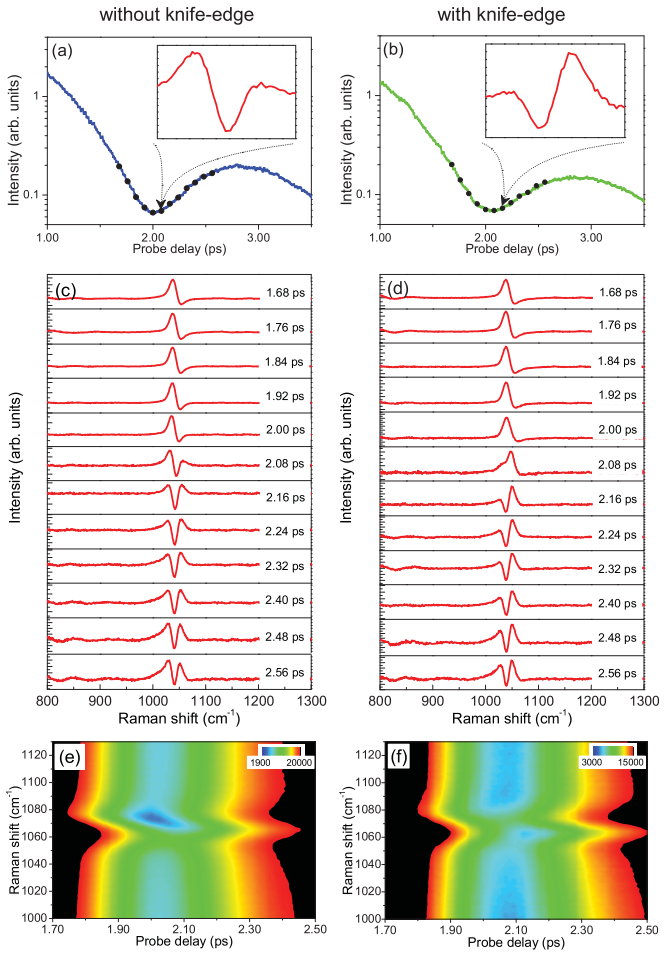

FIG. 3. (Color online) Intensity of the experimental CARS spectra of a methanol aqueous solution with and without the knife edge inserted into the pulse shaper. (a) and (b) show the temporal shapes of the probe pulse in the logarithmic scale, and their insets show the spectrum of the CARS intensity for the probe pulse delays shown. (c) and (d) show the CARS spectrum at many different delays marked as the black dots on the temporal shapes shown in (a) and (b). (e) and (f) show the temporal evolution of the CARS intensity spectrum (without rescaling) as a function of probe delay. In (a)–(d), the spectra are rescaled as $S_{\mathrm{CARS}}(\omega)/S_{\mathrm{BG}}(\omega)$ and $S_{\mathrm{BG}}(\omega)$ is obtained through fitting.

For the case of a weak resonant signal, so that $|P_{\mathrm{BG}}(\omega)| \gg |P_R(\omega)|$, the normalized CARS signal can be written as

$$\frac{S_{\mathrm{CARS}}(\omega,\phi)}{S_{\mathrm{BG}}(\omega,\phi)} \approx 1 + \frac{2\,\mathrm{Re}[e^{i\phi}P_R^*(\omega,\phi)]}{|P_{\mathrm{BG}}(\omega,\phi)|}.$$

Although this condition is not well satisfied in the present work, it is easily satisfied for materials with small Raman cross sections or in low concentrations [11]. The real part of $\chi_R^{(3)}(\omega)$ can then be obtained when $\phi = 0$ or $\pm\pi$. Similarly, once we can find the probe delay corresponding to $\phi = \pi/2$, the imaginary part can be obtained through

$$\frac{S_{\mathrm{CARS}}(\omega,\pi/2)}{S_{\mathrm{BG}}(\omega,\pi/2)} \approx 1 + \frac{2\,\mathrm{Im}\,[P_R(\omega,\pi/2)]}{|P_{\mathrm{BG}}(\omega,\pi/2)|}.$$

The experimental CARS spectra with knife edge shown in Fig. 3(d) approximately reveals the real part ($\tau = 1.68$ ps) and

imaginary part ($\tau = 2.08$ ps) of $\chi_R^{(3)}(\omega)$. We confirm that we can get the imaginary part by observing that its peak frequency is right at the middle of the real curve. Although this is not perfect, we propose that the imaginary curve can be improved by using a delay line with higher resolution to find the exact probe delay for $\phi = \pi/2$.

What this shows is that, in general, the gradual changes in the spectral pattern measured as the probe delay (and therefore the phase ϕ) is varied will reveal the phase information within the Raman spectrum.

Regarding the relative intensity between the resonant and FWM fields, we observe that the probe intensity at the nodes with more asymmetry in Fig. 3(b) is larger than that in Fig. 3(a). The intensities of the Raman line with knife edge, both at 2.02 and 2.08 ps, are weaker than that without knife edge due to the energy loss when the probe spectrum is cut; nevertheless, the intensities of the FWM background are stronger. The contrast ratios of the resonant signal to FWM are 0.71 (without knife edge at 2.02 ps), 0.65, and 0.39 (with knife edge at 2.02 and 2.08 ps, respectively). The lowest intensity of the resonant signal is around 2000 counts. Compared to the double-quadrature spectral interferometry CARS [17] where pure methanol was used in a shorter acquisition time (10 ms), our method has similar sensitivity but no obvious noise.

In conclusion, we have demonstrated a self-implemented heterodyne CARS by using its intrinsic FWM background as the local oscillator. Our configuration uses two broadband Gaussian preparatory pulses and a time-delayed narrow-band probe pulse. We introduce an imaginary component to the probe field in the time domain by inserting a knife edge before the focal plane of a $4f$ pulse shaper, thereby breaking the symmetry of the top-hat-like spectrum. Since the FWM instantaneously responds to the temporal overlap of the preparatory and the probe pulses, it undergoes a gradual phase shift by π when the preparatory pulses cross the node of the real part of the probe field. Due to vibrational coherence, the resonant Raman signal is somewhat insensitive to the overlapping time near the node. We observe the shape changes of the Raman line from aqueous methanol solution, and we directly observe the imaginary part of $\chi_R^{(3)}$ when the phase of the FWM equals $\pi/2$. We also show that more asymmetry of probe spectrum produces a stronger probe field (and thus FWM) at the node by comparing the experimental results from two different probe spectra. Therefore, we have the flexibility to control both the relative phase between the resonant Raman and FWM fields by adjusting the probe delay and the relative amplitude by modifying the probe spectrum.

We thank Dr. Marlan O. Scully, Dr. Aleksei M. Zheltikov, and Dr. Qingqing Sun for helpful discussions and acknowledge support from Aretais Inc., the Office of Naval Research, the National Science Foundation (Grants No. PHY 354897 and No. 722800), the Texas Advanced Research Program (Grant No. 010366-0001-2007), the Army Research Office (Grant No. W911NF-07-1-0475), and the Robert A. Welch Foundation (Grant No. A1547).

[1] G. L. Eesley, *Coherent Raman Spectroscopy* (Pergamon, New York, 1981).

[2] G. I. Petrov, R. Arora, V. V. Yakovlev, X. Wang, A. V. Sokolov, and M. O. Scully, Proc. Natl. Acad. Sci. USA **104**, 7776 (2007).

[3] D. Pestov, G. O. Ariunbold, X. Wang, R. K. Murawski, V. A. Sautenkov, A. V. Sokolov, and M. O. Scully, Opt. Lett. **32**, 1725 (2007).

[4] J.-L. Oudar, R. W. Smith, and Y. R. Shen, Appl. Phys. Lett. **34**, 758 (1979).

[5] J.-X. Cheng, L. D. Book, and X. S. Xie, Opt. Lett. **26**, 1341 (2001).

[6] A. Volkmer, L. D. Book, and X. S. Xie, Appl. Phys. Lett. **80**, 1505 (2002).

[7] D. Pestov, X. Wang, R. K. Murawski, G. O. Ariunbold, V. A. Sautenkov, and A. V. Sokolov, J. Opt. Soc. Am. B **25**, 768 (2008).

[8] B. Yellampalle, R. D. Averitt, A. Efimov, and A. J. Taylor, Opt. Express **13**, 7672 (2005).

[9] T. A. H. M. Scholten, G. W. Lucassen, F. F. M. De Mul, and J. Greve, Appl. Opt. **28**, 1387 (1989).

[10] D. Pestov, R. K. Murawski, G. O. Ariunbold, X. Wang, M. Zhi, A. V. Sokolov, V. A. Sautenkov, Y. V. Rostovtsev, A. Dogariu, Y. Huang, and M. O. Scully, Science **316**, 265 (2007).

[11] X. Wang, A. Zhang, M. Zhi, A. V. Sokolov, and G. R. Welch, Phys. Rev. A **81**, 013813 (2010).

[12] X. Wang, A. Zhang, M. Zhi, A. V. Sokolov, G. R. Welch, and M. O. Scully, Opt. Lett. **35**, 721 (2010).

[13] E. O. Potma, C. L. Evans, and X. S. Xie, Opt. Lett. **31**, 241 (2006).

[14] C. L. Evans, E. O. Potma, and X. S. Xie, Opt. Lett. **29**, 2923 (2004).

[15] M. Jurna, J. P. Korterik, C. Otto, J. L. Herek, and H. L. Offerhaus, Opt. Express **16**, 15863 (2008).

[16] C. Müller, T. Buckup, B. von Vacano, and M. Motzkus, J. Raman Spectrosc. **40**, 809 (2009).

[17] S.-H. Lim, A. G. Caster, and S. R. Leone, Phys. Rev. A **72**, 041803(R) (2005).

[18] B. Li, W. S. Warren, and M. C. Fischer, Opt. Express **18**, 25825 (2010).

[19] D. Oron, N. Dudovich, D. Yelin, and Y. Silberberg, Phys. Rev. Lett. **88**, 063004 (2002).